

Phase-field modeling of stress-induced surface instabilities in heteroepitaxial thin films

D. J. Seol,^{a)} S. Y. Hu,^{b)} Z. K. Liu, and L. Q. Chen

Department of Materials Science and Engineering and the Materials Research Institute, The Pennsylvania State University, University Park, Pennsylvania 16802,

S. G. Kim

Department of Materials Science and Engineering, Kunsan National University, Kunsan, 573-360, Korea

K. H. Oh

School of Materials Science and Engineering and Research Institute of Advanced Materials, Seoul National University, San 56-1, Shinrim-dong, Gwanak-gu, Seoul 151-742, Korea

(Received 25 June 2004; accepted 14 June 2005; published online 25 August 2005)

A phase-field model for investigating the surface morphological evolution of a film is developed, taking into account the surface energies of film and substrate, the interfacial energy between the film and substrate, and the elastic energy associated with the lattice mismatch between the film and substrate. Using the lattice mismatch and the surface energies for the Ge/Si heteroepitaxial system, the morphology of islands and the formation of a wetting layer are investigated using two-dimensional simulations. The results show that the wetting angle increases continuously with the increase in the lattice mismatch, and the surface angle of the island on wetting layer varies with the island size. It is demonstrated that the anisotropy of elastic interactions alone is not sufficient to cause surface angle discontinuity or faceting that is observed in experiments. © 2005 American Institute of Physics. [DOI: 10.1063/1.1996856]

I. INTRODUCTION

A nonhydrostatically stressed solid in contact with its own vapor phase can develop morphological instabilities to partially release its elastic energy, leading to a surface roughening and the formation of a three-dimensional (3D) array of islands or quantum dot structures.¹⁻³ Several analytical approaches have been proposed based on a surface evolution equation, taking into account the mass transport, surface, and elastic energy.⁴⁻⁷ There have also been a number of phase-field models developed for predicting the morphological evolution of a stressed solid in contact with its melt,⁸ the surface instability of heteroepitaxial films,^{9,10} and the effect of misfitting dislocations on surface morphologies.¹¹ Numerical simulations by coupling a kinetic equation with the finite element method (FEM) have also been employed to model the formation of quantum dot structures in heteroepitaxial thin films,^{12,13} where they assume *a priori* the shape of islands or the existence of a wetting layer. Recently, Green's function-based Fourier spectral method has been proposed to study the effect of growth kinetics on surface morphology.¹⁴ The proposed numerical models describe the surface instabilities with two competing factors, the elastic and surface energy. However, the island morphology is strongly dependent on the relative values of the surface energies of the film and substrate, the interfacial energy between the film and substrate as well as the elastic energy associated with the lattice-mismatch strain.

The main purpose of the current study is to present a

phase-field model to describe the surface evolution of a stressed thin film in contact with its vapor phase taking into account the elastic energy, the surface energies, and the interfacial energy. The elastic solution is obtained by considering a multiphase system with different elastic constants in different phases. Our approach does not make any *a priori* assumptions with regard to the final island shape, the ratio of the height to the base length of an island, the distance between islands, and the possible existence of a wetting layer. It is able to predict the formation dynamics, shape, and spatial distribution of island structures with or without a wetting layer from an initially flat film constrained by a substrate through a mismatch strain.

II. PHASE-FIELD MODEL

We consider a cubic thin film grown heteroepitaxially on a cubic substrate. The film undergoes lattice-mismatch-induced surface evolution forming an island structure with or without a wetting layer. We introduce three conserved order parameters, ϕ_1 , ϕ_2 , and ϕ_3 , to represent the volume fractions of gas, film, and substrate phases, respectively (see Fig. 1). The coarse-grained Ginzburg-Landau free energy of the multiphase system, including bulk free energies, surface energies, interfacial energy, and elastic energy, is modeled using the following free-energy functional:

$$F = \int \left[- \sum_{i \neq j}^2 (\alpha_{ij}^2 \nabla \phi_i \cdot \nabla \phi_j + \omega_{ij} \phi_i^2 \phi_j^2) + f^{\text{el}} \right] dV, \quad (1)$$

$$i, j = 1, 2, 3,$$

with $\alpha_{ij} = \alpha_{ji}$, $\omega_{ij} = \omega_{ji}$, and the constraint $\sum_{i=1}^3 \phi_i = 1.0$, where

^{a)}Electronic mail: sxd42@psu.edu

^{b)}Present address: MST8, Los Alamos National Laboratory, Los Alamos, NM 87545.

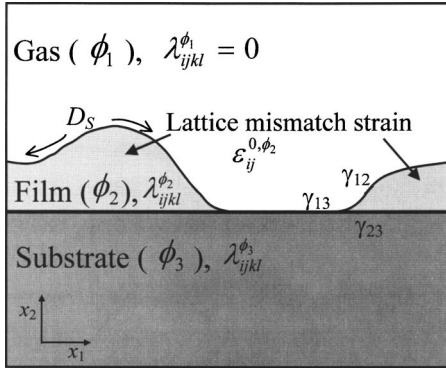


FIG. 1. Schematic illustration of a stressed heteroepitaxial film.

α_{ij} is the gradient energy coefficient, ω_{ij} is the height of double-well potential, and f^{el} is the elastic energy density. We define the elastic constants and eigenstrains as a function of order parameters¹⁵

$$\lambda_{ijkl}(\vec{\mathbf{r}}) = \sum_{p=1}^3 \phi_p(\vec{\mathbf{r}}) \lambda_{ijkl}^{\phi_p} = \lambda_{ijkl}^0 + \sum_{p=1}^3 \phi_p(\vec{\mathbf{r}}) \Delta \lambda_{ijkl}^{\phi_p}, \quad (2)$$

$$\varepsilon_{ij}^0(\vec{\mathbf{r}}) = \sum_{p=1}^3 \phi_p(\vec{\mathbf{r}}) \varepsilon_{ij}^{0,\phi_p}, \quad (3)$$

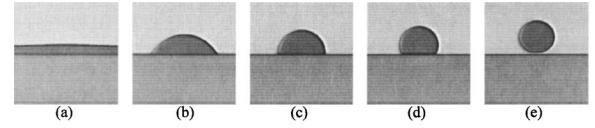
where λ_{ijkl}^0 is the elastic constants of a reference phase, $\varepsilon_{ij}^{0,\phi_p}$ is the eigenstrain of p phase, and $\Delta \lambda_{ijkl}^{\phi_p} = \lambda_{ijkl}^{\phi_p} - \lambda_{ijkl}^0$. Mechanical equilibrium is satisfied when $\sigma_{ij,j} = 0$, where σ_{ij} are the stress components in the film and are given by $\sigma_{ij} = \lambda_{ijkl}(\varepsilon_{kl} - \varepsilon_{kl}^0)$. The total strain $\varepsilon_{kl}(\mathbf{r})$ is separated into homogeneous strain (ε_{ij}) and heterogeneous strain ($\delta \varepsilon_{ij}$), i.e., $\varepsilon_{ij}(\mathbf{r}) = \varepsilon_{ij} + \delta \varepsilon_{ij}(\mathbf{r})$. The homogeneous strain represents the uniform macroscopic strain characterizing the macroscopic shape and the volume change. Thus, the heterogeneous strain satisfies $\int_V \delta \varepsilon_{ij}(\mathbf{r}) d^3 r = 0$. To solve the heterogeneous strain, we introduce a set of displacement $u_i(\mathbf{r})$ through $\delta \varepsilon_{ij}(\mathbf{r}) = \frac{1}{2}(u_{i,j} + u_{j,i})$. The equation of mechanical equilibrium can be written as

$$\left\{ \lambda_{ijkl}^0 \frac{\partial^2}{\partial r_j \partial r_l} + \frac{\partial}{\partial r_j} \left(\sum_p \phi_p \Delta \lambda_{ijkl}^{\phi_p} \right) \frac{\partial}{\partial r_l} \right\} u_k(\mathbf{r}) = \left(\lambda_{ijkl}^0 + \sum_p \phi_p \Delta \lambda_{ijkl}^{\phi_p} \right) \frac{\partial}{\partial r_j} \left(\sum_q \varepsilon_{kl}^{0,\phi_q} \phi_q \right) + \frac{\partial}{\partial r_j} \left(\sum_p \Delta \lambda_{ijkl}^{\phi_p} \phi_p \right) \left(-\varepsilon_{kl} + \sum_q \phi_q \varepsilon_{kl}^{0,\phi_q} \right). \quad (4)$$

The elastic solution for Eq. (4) can be obtained by the iteration method in which the zeroth-order solution in the Fourier space is given by¹⁶

$$u_k^0(\mathbf{g}) = -i G_{ik}(\mathbf{g}) g_j \sum_p (\sigma_{ij}^{0,\phi_p} \phi_p) \mathbf{g}, \quad (5)$$

where g_j is the j th component of a reciprocal lattice vector \mathbf{g} , $G_{ik}(\mathbf{g})$ is the inverse tensor to $[G^{-1}(\mathbf{g})]_{jk} = g^2 \lambda_{ijkl}^0 n_j n_l = g^2 \Omega_{ik}^{-1}(\mathbf{n})$ with $\mathbf{n} = \mathbf{g}/|\mathbf{g}|$, and $\sigma_{ij}^{0,\phi_q} = \lambda_{ijkl}^0 \varepsilon_{kl}^{0,\phi_q}$. The n th order solution in the Fourier space is given by



	a	b	c	d	e
γ_{12} (J/m^2)	1.0	1.0	1.0	1.0	1.0
γ_{13} (J/m^2)	3.0	1.0	1.0	1.0	1.0
γ_{23} (J/m^2)	1.0	0.293	1.0	1.707	3.0
θ (deg)	0 (wetting)	45	90	135	180 (dewetting)

FIG. 2. Morphology of an island near equilibrium and the corresponding surface and interfacial energies.

$$u_k^n(\mathbf{g}) = -i G_{ik}(\mathbf{g}) g_j \left[\sum_p \sigma_{ij}^{0,\phi_p} \phi_p - \sum_p \Delta \sigma_{ij}^{\phi_p} \phi_p + \sum_p \sum_q \Delta \sigma_{ij}^{\phi_p \phi_q} \phi_p \phi_q - \sum_p \phi_p \Delta \lambda_{ijkl}^{\phi_p} \frac{\partial u_k^{n-1}(\mathbf{r})}{\partial r_l} \right] \mathbf{g}, \quad (6)$$

where $\Delta \sigma_{ij}^{\phi_p} = \Delta \lambda_{ijkl}^{\phi_p} \varepsilon_{kl}$ and $\Delta \sigma_{ij}^{\phi_p \phi_q} = \Delta \lambda_{ijkl}^{\phi_p \phi_q} \varepsilon_{kl}^{0,\phi_q}$. The stress and strain fields, and thus, the elastic energy density f^{el} can be calculated from the displacement field in terms of the order parameters.

To simplify the evolution equation, we assume that the phase field (ϕ_3) describing the substrate is static, i.e., it does not evolve with time. Since $\phi_1 + \phi_2 + \phi_3 = 1$, we choose ϕ_2 as the independent phase field and its evolution follows the Cahn–Hilliard equation

$$\frac{\partial \phi_2}{\partial t} = \nabla \cdot \left[M \nabla \frac{\delta F}{\delta \phi_2} \right], \quad (7)$$

where the mobility is given by $M = \phi_1(1 - \phi_1)\mathbf{M}$, \mathbf{M} is the average mobility, and F is the total free energy given in (1).

In the numerical simulations, we rescale the length and time using $\mathbf{r}^* = \mathbf{r}/l_0$ and $t^* = t\mathbf{M}f_0/l_0^2$ where l_0 is a characteristic length scale and f_0 is an energy scale. The evolution equation in the reduced variables is given by

$$\frac{\partial \phi_2}{\partial t^*} = \nabla^* \cdot \left\{ \phi_1(1 - \phi_1) \nabla^* \left[-4\alpha_{12}^{*2} \nabla^{*2} \phi_2 + 2(\alpha_{23}^{*2} - \alpha_{12}^{*2} - \alpha_{31}^{*2}) \nabla^{*2} \phi_3 + 2\omega_{12}^* \phi_1 \phi_2 (\phi_1 - \phi_2) + 2\omega_{23}^* \phi_2 \phi_3^2 - 2\omega_{31}^* \phi_3^2 \phi_1 + f^{*\text{el}} \right] \right\}, \quad (8)$$

where $\nabla^* = l_0 \nabla$, $\alpha_{ij}^* = \alpha_{ij}/f_0 l_0^2$, $\omega_{ij}^* = \omega_{ij}/f_0$, and $f^{*\text{el}} = f^{\text{el}}/f_0$. For numerical stability and efficiency, we employed the semi-implicit Fourier-spectral method for solving the Cahn–Hilliard equation with a variable mobility.¹⁷

III. RESULTS AND DISCUSSION

The surface and/or interfacial energy are related to the gradient energy coefficient and the height of double-well potential as $\gamma_{ij} = \alpha_{ij} \sqrt{2\omega_{ij}}/3$, which is determined from the stationary profile of the phase-field parameter. The effects of surface energies and interfacial energy on the morphology of the island near equilibrium are shown in Fig. 2. The light gray, gray, and dark gray represent the gas, substrate, and the film, respectively. The mismatch strain across the film/

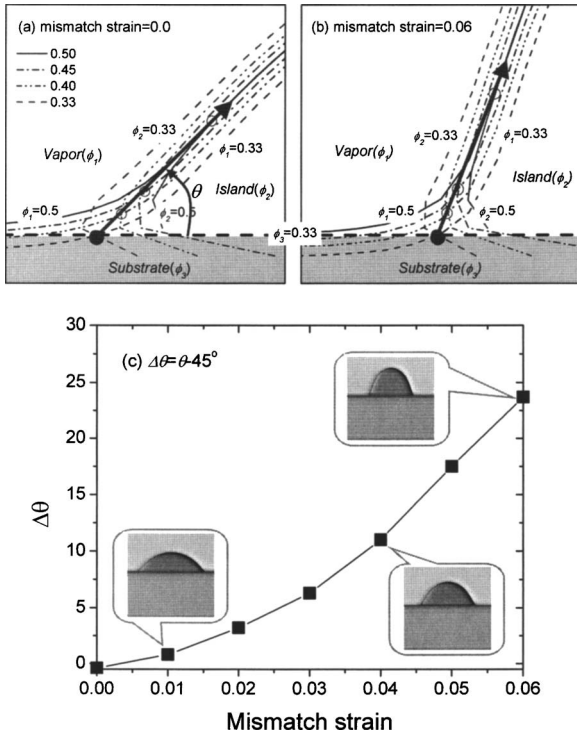


FIG. 3. Change of contact angle with mismatch strain for the case with $\gamma_{12}/\gamma_{13}/\gamma_{23}=1.0/1.0/0.293$. Line contours are drawn of field variables ϕ_1 and ϕ_2 at the values given by the legends, 0.5, 0.45, 0.4, and 0.33. The gray region corresponds to the substrate.

substrate interface is assumed to be zero and the gravity force is not considered here. Using different ratios of the surface energies, γ_{12} and γ_{13} for film and substrate, and the interfacial energy γ_{23} between the film and the substrate, as listed in the table, the film is shown to evolve from an initial hemisphere to various shapes. The simulated contact angles measured from the final shapes for each case agree with the analytical solutions from Young equation, $\gamma_{13}=\gamma_{23}+\gamma_{12}\cos\theta$, within an error range of $\sim 5^\circ$.

As the mismatch strain between film and substrate increases, the elastic energy is found to affect the wetting angle of island. Figures 3(a) and 3(b) are magnified plots around the triple points with the contours of field variables ϕ_1 and ϕ_2 at the values given on the legends, 0.5, 0.45, 0.4, and 0.33. The gray region corresponds to the substrate where $\phi_3 \geq 0.33$. The measured contact angle is the angle between x_1 axis and the line connecting the triple point $\phi_1=\phi_2=\phi_3=1/3$ and the point where $\phi_1=\phi_2=0.5$. Other points marked by circles where $\phi_1=\phi_2$ are approximately on the line. Figure 3(c) shows the change in the equilibrium contact angle as a function of the mismatch strain. The surface energies and interfacial energy are chosen to be 1.0/1.0/0.293 for $\gamma_{12}/\gamma_{13}/\gamma_{23}$, respectively, as the case (b) in Fig. 2, thus $\Delta\theta = \theta_{\text{measured}} - 45^\circ$. It is shown that the lattice-mismatch strain significantly changes the contact angle of the island. This result is contradictory to the sharp interface analysis which compared elastic energy with interfacial energy within a circle of radius R^* centered at the triple point and concluded that the singularity associated with the elastic fields is weaker than that due to the interfacial energy and hence cannot modify the wetting angle in the limit that $R^* \rightarrow 0$.¹⁸ Mi-

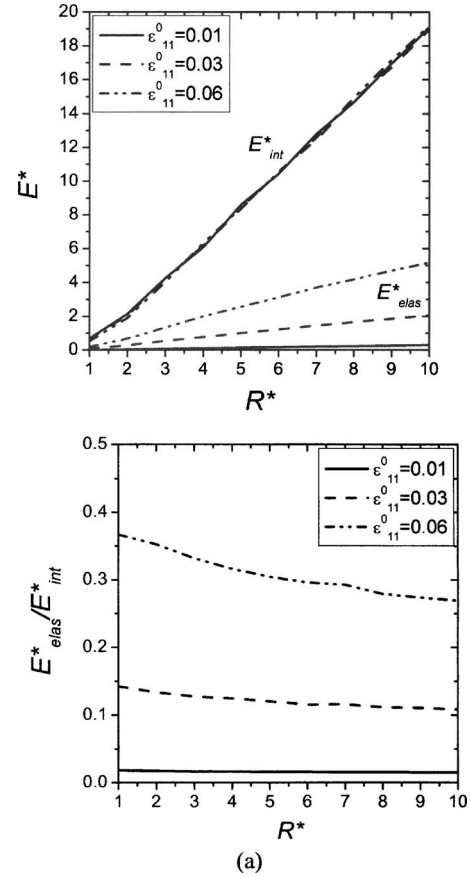


FIG. 4. Variation of (a) interfacial and elastic energies and (b) their ratio within a circle of radius R^* from the triple point.

croscopically, however, the radius should be at least be larger than the lattice constant. In our simulations, the elastic energy E_{elas}^* and the interfacial energy E_{int}^* within the circle of R^* of nanometer size from the triple point are calculated and plotted versus R^* in Fig. 4. We can see that E_{elas}^* and E_{int}^* are comparable, and the ratio E_{elas}^*/E_{int}^* increases with the decrease of R^* , which implies a stress concentration around the triple point. As a consequence, the contact angle increases with the increase of the mismatch strain.

An initially flat film may evolve to an island structure when the strain energy relaxation overcomes the surface energy increase, as observed in many heteroepitaxial films such as $\text{Si}_{1-x}\text{Ge}_x$ on a Si substrate.¹⁹ In order to simulate the morphological evolution of multiple island structure, we use the parameters that correspond to the Ge/Si system. The lattice-mismatch strain is 4% between pure Ge and Si. The surface energies and interfacial energy for (001) epitaxial growth are $\gamma_{12}=1.0 \text{ N m}^{-1}$, $\gamma_{13}=1.5 \text{ N m}^{-1}$,²⁰ and $\gamma_{23}=0.01 \text{ N m}^{-1}$.²¹ The elastic constants are $C_{11}=166 \times 10^9 \text{ N m}^{-2}$, $C_{12}=64.0 \times 10^9 \text{ N m}^{-2}$, and $C_{44}=79.6 \times 10^9 \text{ N m}^{-2}$ for Si, and $C_{11}=126 \times 10^9 \text{ N m}^{-2}$, $C_{12}=44 \times 10^9 \text{ N m}^{-2}$, and $C_{44}=67.7 \times 10^9 \text{ N m}^{-2}$ for Ge, respectively.^{13,22} We define the energy scale following Ref. 15, i.e., $f_0=N_V k_B T$, where N_V is the number of atoms per unit volume, k_B is the Boltzmann constant, and T is the temperature in K, thus f_0 is $\sim 10^9 \text{ N m}^{-2}$ at 1000 K. We used 256×64 discrete grid points and applied periodic boundary conditions along x_1 and x_2 axes. The grid spacing in real space is

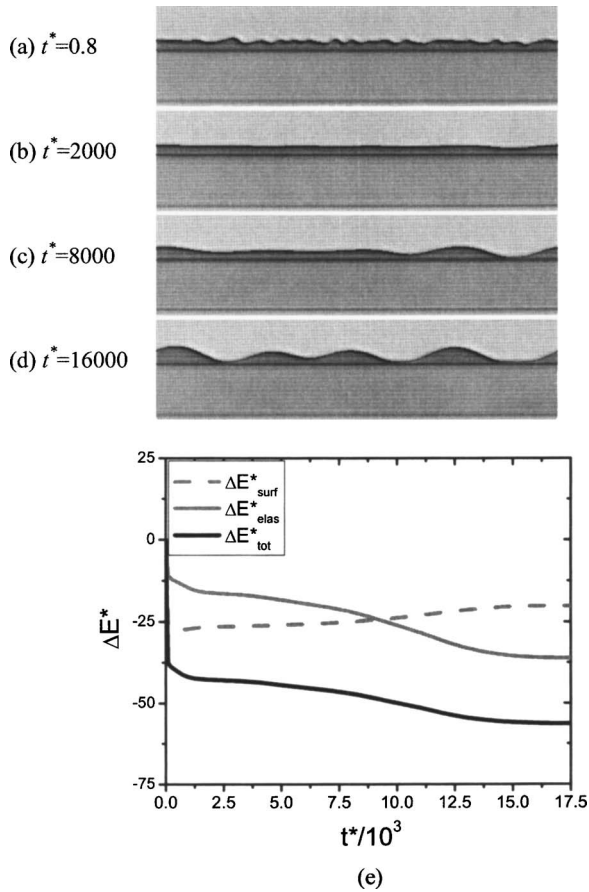


FIG. 5. Temporal evolution of epitaxial Ge film on Si substrate [(a)–(d)] and the corresponding energy changes (e).

chosen to be $\Delta x_1/l_0 = \Delta x_2/l_0 = 1.0$ with the length scale l_0 of 1.0 nm. The time step for integration is $\Delta t^* = 4 \times 10^{-3}$; The initial perturbation of the surface is described by the film thickness $h(x_1)$ using a superposition of p static plane waves with the amplitudes a_m and wave numbers k_m , $h(x_1) = h_0 + \sum_{m=1}^p a_m \sin(k_m x + \varphi_m)$, where h_0 is the average film thickness, φ_m the initial phase of the m th wave within the range $\varphi_m \in [0, 2\pi]$, and the index m the number of the wavemodes.⁹ The wave number is $k_m = 2\pi m/L$, where L is the domain length in the x_1 direction. We used 32 waves with $h_0 = 6l_0$ and $a_m = 0.25l_0$ for all waves to describe the initial thickness profile. Figures 5(a)–5(d) show the temporal evolution of a stressed Ge film on a Si substrate, and the corresponding energy changes, $\Delta E^* = E_{t^*} - E_{t^*=0}$, are plotted in Fig. 5(e). It can be seen that the surface perturbations with high frequencies decay rapidly at the initial stage, driven by the decrease in the surface energy ΔE_{surf}^* . Islands form gradually to relax the elastic energy. The base lengths of the islands observed in Fig. 5(d) are about 43–55 nm, which, despite the two-dimensional nature of simulations, are surprisingly similar to the experimentally measured values of Ge islands on Si before the coarsening stage begins.²³ The ratio of the height to the length of islands is 0.17–0.19 which is similar to the limiting value of 0.18 observed in chemical-vapor deposition.²⁴ However, it is much larger than that of hut structures,²⁵ but is smaller than equilibrium values which can be as large as 0.3.²⁶

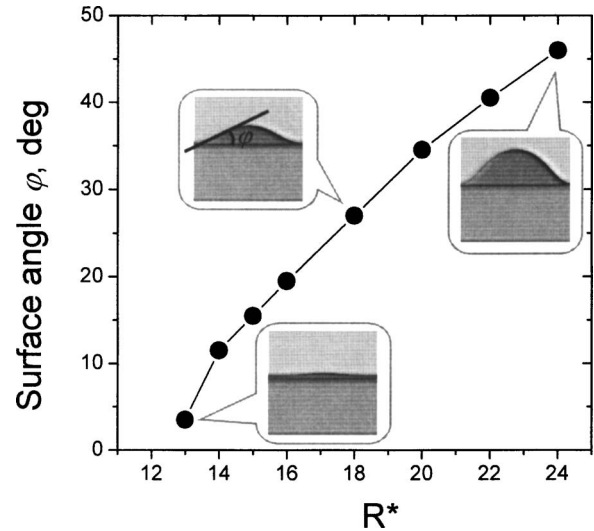


FIG. 6. The variation of surface angles of a single Ge island with size.

Since there exists a wetting layer, the surface angle is defined as the angle that the extrapolated surface line where $\phi_1 = \phi_2 = 0.5$ makes with the substrate, as indicated by φ in Fig. 6. Considering the fact that the elastic energy is proportional to the island volume, the island size is likely to affect the surface angle for a given lattice mismatch. To study the effect of island size on the surface angle, we simulated the time evolution of a single island with various sizes. An initial hemisphere with the radius R^* on the substrate evolves to form the wetting layer quickly to reduce the interfacial energy, and the surface maintains a certain angle with the substrate where the total energy of the system is minimized. The measured surface angles are plotted in Fig. 6 with respect to R^* along with the morphologies. It is found that the surface angle increases with the increase in R^* . From the dependence of wetting angles and surface angles on the elastic energy, we can conclude that the anisotropy in elastic interactions alone is not sufficient to produce the faceting of islands which is observed in experiments. To understand the formation of the specific facet angles, the phase-field model needs to be extended to include the anisotropy in surface energies and surface stresses that are believed to be responsible for faceting.^{27–32}

IV. CONCLUSIONS

A phase-field model is developed for predicting the stress-induced instabilities of a solid film in contact with a gas phase and constrained by a substrate. It solves the elasticity equation using an efficient iterative method and allows different relative values of surface energies and interfacial energy. The model can be employed to predict the island shape, spatial distribution as well as their temporal evolution with or without a wetting layer. It is shown that the lattice mismatch has a significant effect on the wetting angle of islands on a substrate, and the surface angle of the island on wetting layer depends on the island size for a given lattice mismatch. The results demonstrate that the elastic energy results in continuous changes in wetting angles and surface angles. The model will be extended to include the surface

energy anisotropy and the surface stress anisotropy for studying the faceting of island surfaces in the future.

ACKNOWLEDGMENTS

The authors gratefully acknowledge the financial support of NSF under the Grant No. DMR0122638 and the Postdoctoral Fellowship Program of Korea Science and Engineering Foundation (KOSEF).

- ¹R. J. Asaro and W. A. Tiller, *Metall. Trans.* **3**, 1789 (1971).
- ²M. A. Grinfeld, *Sov. Phys. Dokl.* **31**, 831 (1986).
- ³D. J. Srolovitz, *Acta Metall.* **37**, 621 (1989).
- ⁴B. J. Spencer, P. W. Voorhees, and S. H. Davis, *Phys. Rev. Lett.* **67**, 3696 (1991).
- ⁵J. E. Guyer and P. W. Voorhees, *Phys. Rev. Lett.* **74**, 4031 (1995).
- ⁶B. J. Spencer, P. W. Voorhees, and J. Tersoff, *Phys. Rev. B* **64**, 235318 (2001).
- ⁷Z. F. Huang and R. C. Desai, *Phys. Rev. B* **65**, 195421 (2002).
- ⁸J. Müller and M. Grant, *Phys. Rev. Lett.* **82**, 1736 (1999).
- ⁹Y. U. Wang, Y. M. Jin, and A. G. Khachatryan, *Acta Mater.* **52**, 81 (2004).
- ¹⁰J. J. Eggleston and P. W. Voorhees, *Appl. Phys. Lett.* **80**, 306 (2002).
- ¹¹M. Haataja, J. Müller, A. D. Rutenberg, and M. Grant, *Phys. Rev. B* **65**, 165414 (2002).
- ¹²P. Liu, Y. W. Zhang, and C. Lu, *Appl. Phys. Lett.* **80**, 3910 (2002).
- ¹³Q. X. Pei, C. Lu, and Y. Y. Wang, *J. Appl. Phys.* **93**, 1487 (2003).
- ¹⁴A. Ramasubramaniam and V. B. Shenoy, *J. Appl. Phys.* **95**, 7813 (2004).
- ¹⁵D. J. Seol, S. Y. Hu, K. H. Oh, and L. Q. Chen, *Met. Mater-Int.* (to be published).
- ¹⁶S. Y. Hu and L. Q. Chen, *Acta Mater.* **49**, 1879 (2001).
- ¹⁷J. Zhu, L. Q. Chen, J. Shen, and V. Tikare, *Phys. Rev. E* **60**, 3564 (1999).
- ¹⁸D. J. Srolovitz and S. H. Davis, *Acta Mater.* **49**, 1005 (2001).
- ¹⁹P. Sutter and M. G. Lagally, *Phys. Rev. Lett.* **84**, 4637 (2000).
- ²⁰A. A. Stekolnikov, J. Furthmüller, and F. Bechstedt, *Phys. Rev. B* **68**, 205306 (2003).
- ²¹S. Ciraci and I. P. Batra, *Phys. Rev. B* **38**, 1835 (1988).
- ²²S. P. Nikanorov, Y. A. Burenkov, and A. V. Stepanov, *Sov. Phys. Solid State* **13**, 2516 (1971).
- ²³F. M. Ross, J. Tersoff, and R. M. Tromp, *Phys. Rev. Lett.* **80**, 984 (1998).
- ²⁴T. I. Kamins, E. C. Carr, R. S. Williams, and S. J. Rosner, *J. Appl. Phys.* **81**, 211 (1997).
- ²⁵Y.-W. Mo, D. E. Savage, B. S. Swartzentruber, and M. G. Lagally, *Phys. Rev. Lett.* **65**, 1020 (1990).
- ²⁶M. Goryll, L. Vescan, K. Schmidt, S. Mesters, H. Lüth, and K. Szot, *Appl. Phys. Lett.* **71**, 410 (1997).
- ²⁷E. Sutter, P. Sutter, P. Zahl, P. Rugheimer, and M. G. Lagally, *Surf. Sci.* **532–535**, 785 (2003).
- ²⁸Y. Zhang, M. Floyd, J. Drucker, and G. L. Kellogg, *J. Appl. Phys.* **90**, 4748 (2001).
- ²⁹V. A. Shchukin, N. N. Ledentsov, P. S. Kop'ev, and D. Bimberg, *Phys. Rev. Lett.* **75**, 2968 (1995).
- ³⁰N. Moll, M. Scheffler, and E. Pehlke, *Phys. Rev. B* **58**, 4566 (1998).
- ³¹P. Raiteri, D. B. Migas, L. Miglio, A. Rastelli, and H. von Känel, *Phys. Rev. Lett.* **88**, 256103 (2002).
- ³²J. Tersoff, B. J. Spencer, A. Rastelli, and H. von Känel, *Phys. Rev. Lett.* **89**, 196104 (2002).